



VICTORIA UNIVERSITY
MELBOURNE AUSTRALIA

Synthesizing dual-track road elevation data

This is the Accepted version of the following publication

Lamb, Matthew and Rouillard, Vincent (2021) Synthesizing dual-track road elevation data. *Probabilistic Engineering Mechanics*, 66. ISSN 0266-8920

The publisher's official version can be found at
<https://www.sciencedirect.com/science/article/pii/S0266892021000527?via%3Dihub>
Note that access to this version may require subscription.

Downloaded from VU Research Repository <https://vuir.vu.edu.au/42925/>

Synthesizing dual-track road elevation data

M.J Lamb (PhD.)^{a*} and V. Rouillard^b (PhD.)

^{a,b}Mechanical Engineering, Victoria University, Footscray Park Campus

PO Box 14428, MCMC 8001 Melbourne, Australia

^{a*}Corresponding Author Email: matthew.lamb@vu.edu.au

Abstract

The ability to synthesize dual-track road elevation profiles enables the multi-axial motion (heave, pitch and roll) of road vehicles to be simulated and investigated. It is important that the synthesized elevation profiles along two wheel tracks, namely kerb-side and driver-side, retain the random and nonstationary character of real roads. The paper introduces a novel method for synthesizing dual-track longitudinal pavement elevation profiles that retain the important statistical characteristics of measured elevation data. Using road profile data from some 400 km of asphalted roads, it was found that variations in the roughness of a single track are well described by the three-parameter Weibull probability distribution function. The location and shape parameters of the distribution were shown to be largely independent to road roughness, leaving the scale parameter as the main index to define the roughness distribution. This led to the creation of a new roughness classification scheme that better represents the roughness range encountered on sealed asphalt roads in modern road networks. The relationship between the driver-side and kerb-side tracks was investigated by analysing the ratio of the roughness and the coherence function between the track profiles. The distributions of the roughness ratio and the coherence function were both found to be independent of overall road roughness and well-defined by the three-parameter Weibull distribution. In the novel method, a random sequence of roughness values for the kerb-side track of the synthesized road is generated with a linear congruential generator from the Weibull distribution, according to the proposed classification. The roughness level of the driver-side track is set according to the distribution function of the driver-side to kerb-side roughness ratio. The elevation Power Spectral Density (PSD) functions of the kerb-side and driver-side tracks are correlated using the coherence function which is also made to vary randomly along the synthesized road. Short stationary segments of the elevation signals are then synthesized from the kerb-side and driver-side PSD functions and concatenated to create two parallel track elevation profiles that are truly nonstationary and emulate the natural (random) fluctuations in road roughness and dual track coherence that are found to exist on real roads.

Keywords: nonstationary, road synthesis, multi-axial, vehicle simulation, IRI

INTRODUCTION

Numerical simulation and laboratory-based testing are becoming an increasingly important aspect of ground vehicle design and evaluation [1]. They enable vehicles to be designed to withstand the stresses associated with dynamic interaction between the vehicle and the uneven road surface, to maintain sufficient forces between the tyres and the road surface ensuring control of the vehicle and to achieve suitable ride conditions for the occupants and cargo. The usefulness of the simulations relies heavily upon the accurate synthesis of the environmental loads applied to the vehicle, particularly road unevenness [1].

Longitudinal road unevenness (profiles) have long been recognized to be random and are generally represented by an elevation power spectral density (PSD) function [2-4]. Artificial longitudinal road profiles can be synthesized by combining the desired PSD functions with a corresponding (uniformly-distributed) random phase spectrum using, for instance, the inverse Fourier transform. This approach invariably produces a random signal that conforms to the Gaussian distribution in accordance with the central limit theorem. This is acceptable when the aim is to create a statistically stationary (constant root-mean-square) road profile signal. However, in reality, such roads do not exist as the localized roughness varies (randomly) long the length of the road. It is, therefore, desirable to synthesize realistic road profiles that include these natural variations in roughness. Such an approach was first broached by Rouillard et al. [5] who treated the longitudinal road profile as a nonstationary process and used a random amplitude modulation function to stochastically alter the root-mean-square (rms) level of the synthesized road profile in accordance with a statistical distribution of the spatial acceleration rms level. Nonstationary road profile synthesis was also addressed by Steinwolf et al. [6] and Abdullah et al. [7] but these were limited to the insertion of bumps into single-track road elevation data using wavelet analysis. The main limitation of this work is that it is restricted to single-track profile synthesis and does not address how a second, parallel track is to be synthesized. This is important if the response of complete vehicles is to be investigated whether numerically or physically using multi-post road simulators.

Several authors have presented studies related to the synthesis of stationary dual wheel-track excitation records [8 - 14] with the vast majority using the coherence function, γ_{lr}^2 , between the driver-side and kerb-side wheel-tracks to synthesize partially correlated dual track data. Typically, a zero average phase difference is assumed between the driver-side and kerb-side wheel-tracks allowing the coherence function to be used as the frequency response function between the driver-side to kerb-side wheel-tracks for the correlated portion of the signal [8, 9, 11, 12, 14]. By using the coherence function as the frequency response function, the energy in the second signal is suppressed at the shorter wavelengths creating a distortion to the shape of the PSD. This is clearly shown by [12] and needs to be accounted for by adding a non-correlated component to the second signal [8, 12, 14]. This process is most clearly demonstrated by Long [14] as illustrated in Figure 1.

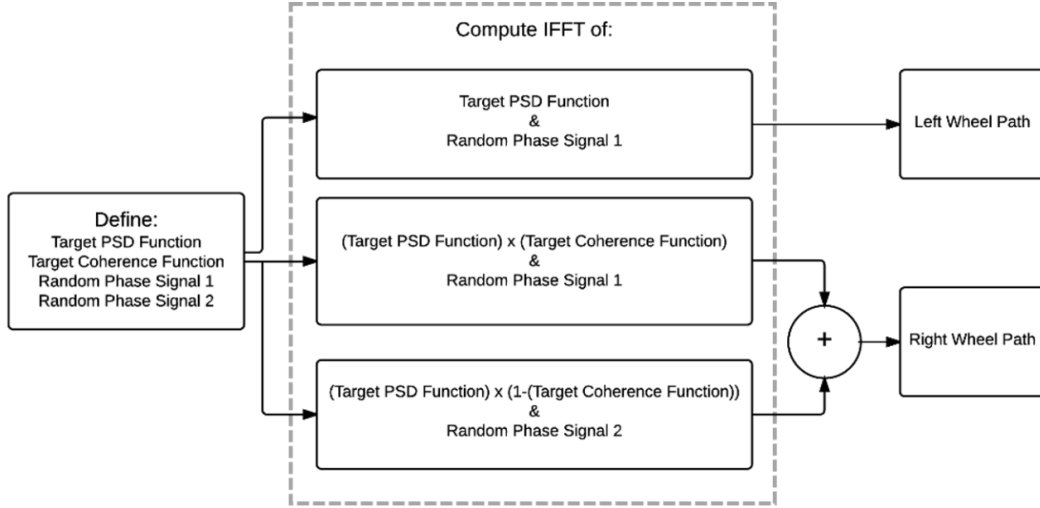


Figure 1: Method for generating correlated dual wheel-track data [14].

One limitation of the process is that it does not account for any difference in roughness that may exist between the driver-side and kerb-side wheel-tracks. Furthermore, despite each of the methods implementing the coherence function to generate the partially correlated tracks, there is no consensus on a suitable coherence model. Although an isotropic assumption is recommended in ISO 8608 [4], it is now broadly accepted that the classic view of roads as an isotropic surface, first proposed by Dodds and Robson [3] then by Kamash and Robson [15], is not adequate [16]. Bogsjö [17] validated coherence models using large road profile records and compared the coherence of measured profiles with the isotropic model. The results showed the isotropic assumption to be inaccurate. A single-parameter exponential model was proposed and was found to accurately describe the coherence spectra of all 20 roads analyzed. Múčka [18] presents a comprehensive overview of the evolution of the various coherence functions that aim at characterizing parallel wheel tracks and found the model proposed by Ammon and Bormann (cited in [18]) to be the most accurate. Unfortunately, the work by Múčka was undertaken on roads of insufficient length. Lamb and Rouillard [19] compared the various models presented by Múčka and found the models of Ammon and Bormann (cited in [18]) and Bogsjö [17] to be accurate. The advantage of the model proposed by Bogsjö is that it can be described using a single (other than measured wheel track) parameter, b_l , as shown in equation (1)

$$\gamma_{lr}^2(n, \rho) = e^{-2\rho b_l n} \quad n = \frac{\Omega}{2\pi} \quad (1)$$

Where n is the spatial frequency in cycles per metre, Ω the angular spatial frequency in radians per metre, ρ the track width in metres and b_l an arbitrary constant.

Lamb and Rouillard [19] investigated the driver-side and kerb-side wheel track relationship further to show that the coherence function varies along the length of the road and should be treated as a nonstationary process. Lamb and Rouillard successfully modelled both the variation in road roughness and the coherence function parameter, b_l , using the Weibull distribution. Analysis of these variations showed that the distribution of the nonstationary coherence function is independent to the roughness level, this is important with regards to the simulation process.

The findings by Lamb and Rouillard demonstrate a further limitation to existing dual wheel-track synthesis methods as none of them consider the road roughness nor the relationship between the kerb-side and driver-side wheel tracks as being nonstationary. The aim of this paper is to develop an easy-

to-implement dual wheel track synthesis procedure which allows for the generation of nonstationary longitudinal profiles that are representative of real roads.

METHOD

The research undertaken by Lamb and Rouillard [19] has provided an indication of typical roughness distributions, a suitable coherence function model and a descriptor of the variation in the coherence function along the length of the road. The finding that the road roughness levels and variations in the coherence function are independent is also significant as it allows their randomisation to be set independently using the associated statistical distribution functions. The work by Lamb and Rouillard is extended here to allow for the simulation of nonstationary dual track data. Specifically this requires methods to:

1. Set the nominal roughness for the road to be simulated
2. Set the roughness variation (distribution) for each wheel track
3. Set coherence relationship between the driver-side and kerb-side wheel tracks.
4. Create the nonstationary dual wheel track profiles

Setting nominal roughness

Typically, overall road roughness is defined using the PSD function of a measured road and is classified in accordance with the ISO-8608 standard [4]. The ISO-8608 standard provides classifications ranging from very smooth (class A) to extremely rough (class H) over eight distinct classes according to (2):

$$G_d(\Omega) = G_d(\Omega_o) \cdot \left(\frac{\Omega}{\Omega_o} \right)^{-w} \quad (2)$$

, where:

- G_d is the displacement PSD (m^3/rad)
- Ω is the angular spatial frequency (rad/m)
- Ω_o is the reference angular spatial frequency (1 rad/m in the standard)
- w is the PSD fitting exponent ($w = 2$ according to the standard)¹

Each road class represents a band of roughness levels which are defined using a geometrical scale as shown in Table 1 (for $w = 2$).

Table 1: ISO-8608 road class degrees of roughness [4]

Road class	$G_d(\Omega_o)$ [$10^{-6} \text{ m}^3/\text{rad}$]		
	Lower limit	Mean	Upper limit
A	-	1	2
B	2	4	8
C	8	16	32
D	32	64	128
E	128	256	512
F	512	1024	2048
G	2048	4096	8192

¹ Arguments for different values for the spectral exponent, w , and for different spectral shape are numerous but, as this is not the focus of this paper, the simple spectral model as contained in ISO 8608 will be used here.

H	8192	16384	32768
----------	------	-------	-------

$$\Omega_o = 1 \text{ rad/m}$$

Research has shown [20] has shown that, for modern, sealed road networks, the majority of roads fall between class A and C making the use of the ISO class approach for characterising and synthesizing sealed roads for modern road networks rather coarse and imprecise. A popular alternative for the definition of road roughness is the international road roughness index (IRI) [21-23] which is not only able to provide an overall roughness for an entire road, but also near-instantaneous (or short distance) estimates along the segment of road. This approach provides the added advantage of not only being useful for estimating the overall (average) roughness of the road, but also the distribution of the road roughness along its length. One limitation of the approach is that it does not provide information on the spectral character of the road surface.

Since both classification indices are widely used, there has been a number of works published on the relationship (3) between the two techniques [24 - 26]. Specifically, work by Kropáč and Múčka [25] has shown that, when $w = 2$,

$$IRI = 2.21 \sqrt{G_d(\Omega_o) / 10^{-6}} \text{ m / km} \quad (3)$$

This relationship has been tested and validated by the authors using synthesized stationary roads. Other authors, including Pawar et. al [26] have also tested and approved the conversion.

Modelling roughness variations

The concept of modelling and synthesizing more realistic road elevation data by introducing random fluctuations in roughness along the length of the road was first introduced by Rouillard et al. [5]. Rouillard et al. used a random amplitude modulation function to stochastically alter the level of a single synthesized wheel-track according to an offset Rayleigh distribution. Lamb and Rouillard [19] extended on this work in an attempt to classify the roughness of dual wheel-track road elevation data. Through the analysis of a wide variety of sealed roads (approximately 400 km in total) in Australia², Lamb and Rouillard showed the roughness distribution for three groupings of roads which may be considered as typical low, moderate and high roughness based on their overall IRI values. The data used in their study included 19 independent elevation data sets (totaling approximately 400 km) measured using an inertial profilometer along a wide variety of sealed asphalted roads across the state of Victoria in Australia. Table 2 lists the details of each elevation data set used by Lamb and Rouillard including an estimate of their overall roughness which is described using IRI. Each data set was measured across a track width of 1.5 m.

Table 2. Validation data set details [19].

Road Name	Road Type	Length [km]	IRI [m/km]		
			Kerb-side	Driver-side	Mean
Princes Hwy East (1A)	Metro. Highway	22.9	1.7	1.7	1.7
Princes Hwy East (2A)	Metro. Highway	20.3	1.5	1.4	1.5
Princes Hwy East (3A)	Metro. Highway	3.3	1.7	1.6	1.7
Princes Hwy East (3B)	Metro. Highway	3.4	2.3	1.8	2.1
Murray Valley Hwy (4A)	Country Highway	47.7	1.9	1.7	1.8

² The authors acknowledge VicRoads, Australia for supplying road elevation data.

Murray Valley Hwy (4B)	Country Highway	43.8	1.6	1.4	1.5
South Gippsland Hwy (3A)	Country Highway	11.3	2.3	2.0	2.2
South Gippsland Hwy (3B)	Country Highway	21.8	2.6	2.1	2.4
South Gippsland Hwy (3C)	Country Highway	15.0	3.1	2.6	2.9
Midland Hwy	Country Highway	14.0	3.3	3.2	3.3
South Gippsland Hwy (5B)	Country Highway	60.8	3.6	3.3	3.5
Daylesford - Malmsbury Rd	Country Road	25.4	4.0	3.3	3.7
Northern Hwy	Country Highway	5.0	4.1	3.8	4.0
Lismore - Skipton Rd	Country Road	32.6	4.2	3.7	4.0
Bendigo - Maryborough Rd	Country Road	22.3	4.3	3.8	4.1
Wiltshire Lane	Country Road	2.3	4.2	4.1	4.2
Pyrenees Hwy	Country Highway	12.4	4.8	4.2	4.5
Timboon - Port Campbell Rd	Country Road	8.0	6.3	4.3	5.3
Euroa - Mansfield Rd	Country Road	8.3	6.1	5.0	5.6

In order to quantify and statistically analyse variations in roughness along the length of the road (nonstationarity) - and taking into account the longest relevant wavelength - data sets of considerable lengths are needed. Therefore, to enable such analysis, a number of records listed in Table 2 were concatenated to produce longer records. Lamb and Rouillard [19], grouped roads of similar average roughness levels together and four roads were created according to their nominal (IRI) roughness.

Road 1: Roads with a mean IRI of 2.1 or less (141.5 km)

Road 2: Roads with a mean IRI of between 2.2 and 3.6 (123.5 km)

Road 3: Roads with a mean IRI of 3.7 or more (116.8 km)

Road 4: Entire data set (381.8 km)

Prior to concatenating the records, a high-pass filter (fourth order Butterworth set at $1/33 \text{ m}^{-1}$) was applied to each segment in order to ensure that the long wavelength errors, that are inherent to inertial profilometers [27], were removed from the data.

The data used by Lamb and Rouillard included roads with average IRI values ranging from 1.5 m/km to 6 m/km, which according to available literature [20, 28], covers the expected range for sealed roads. The IRI distribution for the kerb-side (left in this case) wheel track for 100 m segments is shown in Figure 2.

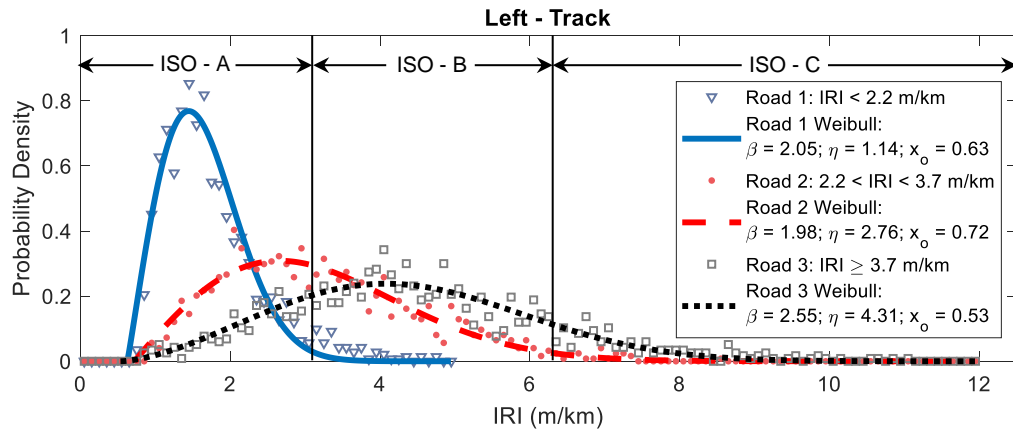


Figure 2: Typical distributions (probability density function) of road roughness (IRI) (edited from [19]).

Lamb and Rouillard modelled the distributions using the three parameter Weibull function (4) [29]:

$$f(x) = \frac{\beta}{\eta} \left(\frac{x - x_o}{\eta} \right)^{\beta-1} \cdot e^{-\left(\frac{x - x_o}{\eta} \right)^\beta} \quad (4)$$

, where:

- The location parameter, x_o , represents the lower bound of the distribution
- The shape parameter, β , influences the overall shape of the function
- The scale parameter, η , sets the breadth of the distribution.

The influence of these three parameters is shown graphically in Figure 3.

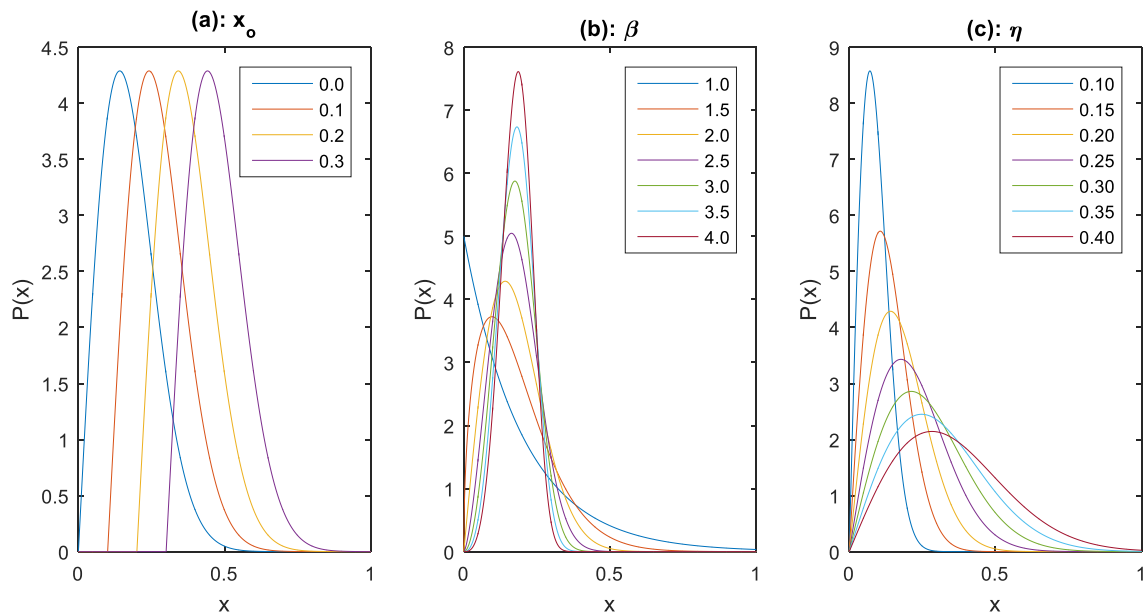


Figure 3 Parameter influence on the Weibull distribution: (a): Location parameter; (b) Shape parameter; (c): Scale parameter.

Use of the Weibull function allows the (nonstationary) roughness of each road type to be easily characterised using only three parameters. These IRI distribution functions, or any distribution function measured by the user, can be exploited to simulate the nonstationary road elevation profiles by using a suitable random number generator. From Figure 2 it can be seen that for the three roads (low, moderate and high overall roughness), both the location and the shape parameters vary little in comparison with the scale parameter regardless of overall roughness. In an attempt to simplify the model, the location and shape parameters were fixed to match the respective means (namely $x_o = 0.625$ and $\beta = 2.20$) and the Weibull distribution was re-fitted to extract the corresponding scale parameters. Adjusting the scale while holding shape and location constant alters the breadth of the fit. In addition, since the area under the model is a constant (one), the maximum value of the probability density will alter. This makes the scale parameter a very useful tool for adjusting the model to suit the roughness range.

The results, shown in Figure 4, reveal that no significant difference is produced when the model is simplified to a single parameter (scale). This is significant as it affords the use of a single index to completely describe the roughness (in this case IRI) distribution of any road.

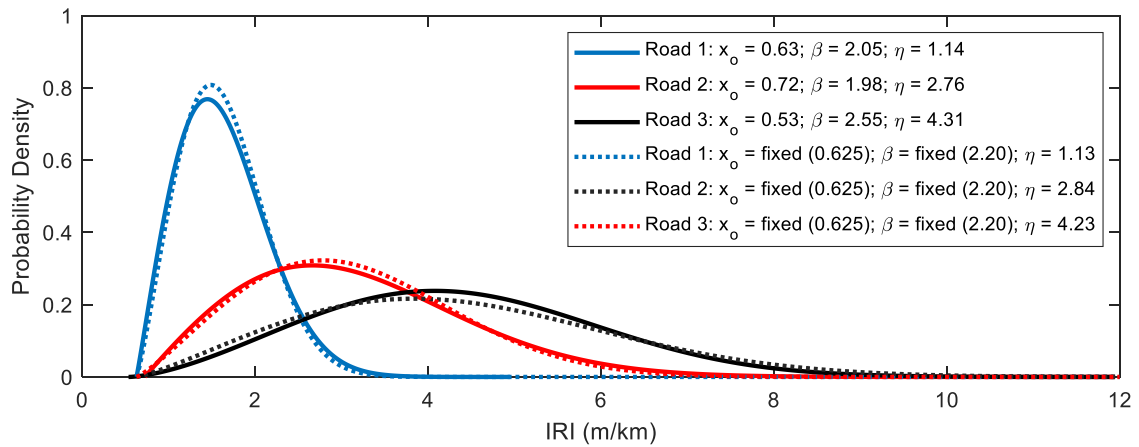


Figure 4: Comparison of the best-fitting Weibull distributions (probability density function) with fixed ($x_o = 0.625$ and $\beta = 2.20$) and variable location and shape parameters.

The statistical properties of the distribution can be determined mathematically using the three Weibull parameters. This is particularly useful as it allows the user to set the scale parameter to achieve the desired mean IRI according to (5) [29], provided that the shape and location parameters have already been set. If the shape and location are set to the values used in Figure 4 (i.e. $x_o = 0.625$ and $\beta = 2.20$), the required shape parameter can be calculated using the simple linear function provided in (6).

$$\eta = \frac{\mu - x_o}{\Gamma\left(1 + \frac{1}{\beta}\right)} \quad (5)$$

$$\eta = 1.13\mu - 0.71 \quad (6)$$

Equations (6) and (3) can be used to relate the distributions to the more familiar ISO standards allowing users to determine an equivalent (at least in terms of the mean) nonstationary road or (6) can be used alone for any desired mean IRI. Selecting an appropriate mean IRI requires knowledge of the type of roads to be simulated and their anticipated roughness levels. According to an extensive global survey of IRI levels on a wide range of roads [20, 28] it is rare for new and rehabilitated roads to have mean IRI values exceeding 3 m/km and in-service roads (which Múčka [20] defines as existing roads) to exceed 8 m/km. Furthermore, according to Múčka [20], the high roughness levels tend to be more prevalent for shorter segments (200 m or less). Mean IRI values of 3 to 8 m/km correspond to the mean roughness for roads of ISO class A to C according to ISO 8608 as illustrated in Figure 2. The distributions shown in Figure 2 also show that, with the exception of very smooth roads (ISO class A), roads are not limited to one ISO class with the variation in IRI increasing with an increase in mean IRI. A new scheme for classifying modern roads is proposed to reflect this. The proposed method is based on the existing ISO classifications which are used to set the overall mean and equation (6) to set the breadth of the roughness distribution. In order to afford better differentiation of roughness, the ISO class band scheme was modified to include intermediate bands. The corresponding values of IRI range, $G_d(\Omega_o)$ and the Weibull scale parameter of these bands are shown in Table 3. In this roughness classification scheme, the lower and upper limits for the IRI are extracted from the Weibull distribution and are fixed to x_o and the 98th percentile (P98) respectively. This means that as overall roughness of a road increases, so does the upper limit and, therefore, the range of IRI values. This is significantly different to the ISO classification scheme used for stationary analysis which treats each roughness band as exclusive to the adjacent bands. The distributions corresponding to Table 3 are presented in Figure 5 which compares each band of the new classification method with roads 1 to 3 of Lamb and Rouillard [19].

Table 3. Proposed roughness classification for modern, sealed, road networks.

Roughness class	IRI [m/km]			$G_d(\Omega_o)$ [10^{-6} m ³ /rad]			η [m/km]
	Lower limit (x_o)	Mean	Upper limit (P98)	Lower limit	Mean	Upper limit (P98)	
0A	0.625	1.56	2.61	0.08	0.50	1.39	1.06
AA		2.21	3.96		1.00	3.21	1.79
AB		3.13	5.88		2.00	7.08	2.82
BB		4.42	8.61		4.00	15.18	4.29
BC		6.25	12.44		8.00	31.69	6.35
CC		8.84	17.89		16.00	65.53	9.28

Note: For all roughness classes $x_o = 0.625$ and $\beta = 2.20$.

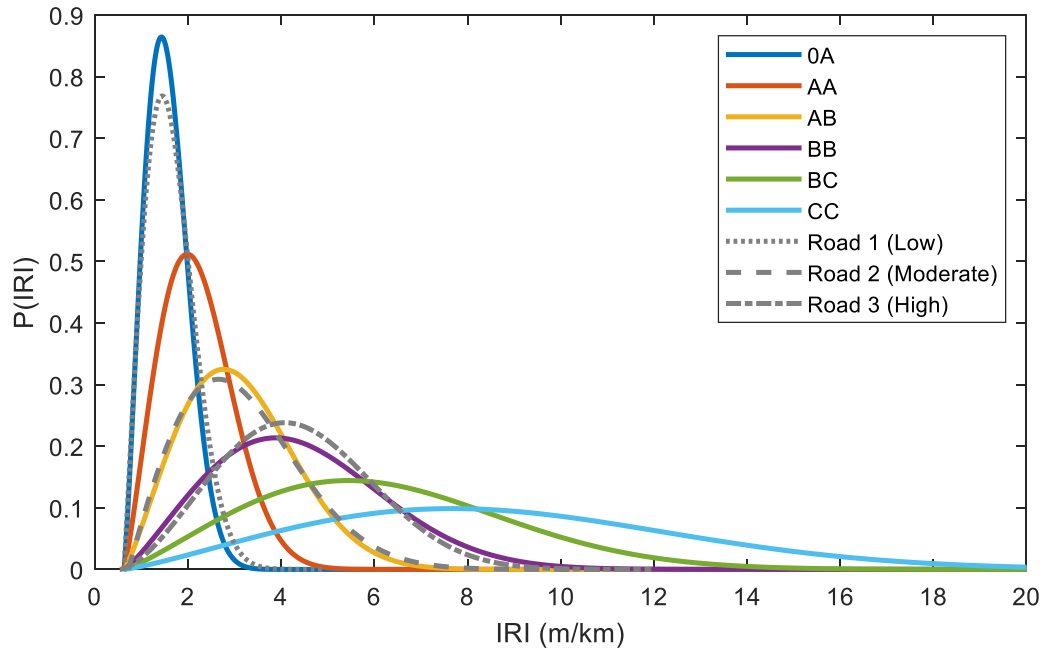


Figure 5: Road roughness distributions for proposed classifications presented in Table 3 with roads 1, 2 and 3 representing the low, moderate and high roughness roads analysed by Lamb and Rouillard [19].

Setting modulated roughness of second wheel-track

It is reasonable to assume that the roughness of the driver-side and kerb-side tracks are not equal for corresponding segments along the road. The relationship between driver-side and kerb-side track roughness is investigated here using the same set of dual track elevation data (roads 1 to 4) used by Lamb and Rouillard [19]. In order to determine the relationship between the driver-side to kerb-side wheel-track roughness ratio of the segment IRI for each track was recorded. This was achieved by calculating the instantaneous IRI values corresponding to each data point in roads 1-4 and applying a 100 m moving average filter before calculating the ratio of the segment IRI of the wheel-tracks. The resulting probability density functions from the analysis are presented in Figure 6 where they are compared to the closest-fitting three-parameter Weibull distribution. Interestingly, the roughness ratio for all cases range from approximately 50% to 150%. The roughness distribution for road 4 (all data) is overlaid on each distribution for comparison purposes. The results show that, for sealed asphalt roads, there is a correlation between the driver-side and kerb-side track roughness with a typical ratio of driver-side roughness to kerb-side roughness of between 0.85 and 0.90. It is also clear that there is no significant variation in the distribution as a function of overall roughness (IRI) and the Weibull fit of all data (i.e. road 4) adequately represents the full range of roads. This allows one distribution (described by only three parameters) to be used to modulate the ratio of driver-side to kerb-side wheel-track roughness to generate realistic, nonstationary dual track elevation profiles. This is achieved by generating a random value of the ratio of driver-side to kerb-side wheel-track roughness in accordance with the Weibull distribution (Figure 6) and multiplying that value by the roughness of the kerb-side wheel-track to obtain the roughness on the driver-side wheel track. One limitation to the results is that they are all gathered from a single track width of 1.5 m. This is seen as a minor limitation as the track width of most vehicles falls between 1.5 m and 2 m. It must also be noted that the roads used in this analysis are all sealed asphalt roads. Further analysis is required for other road types such as Portland

Cement Concrete pavements which may have less variation between the driver-side and kerb-side wheel-tracks.

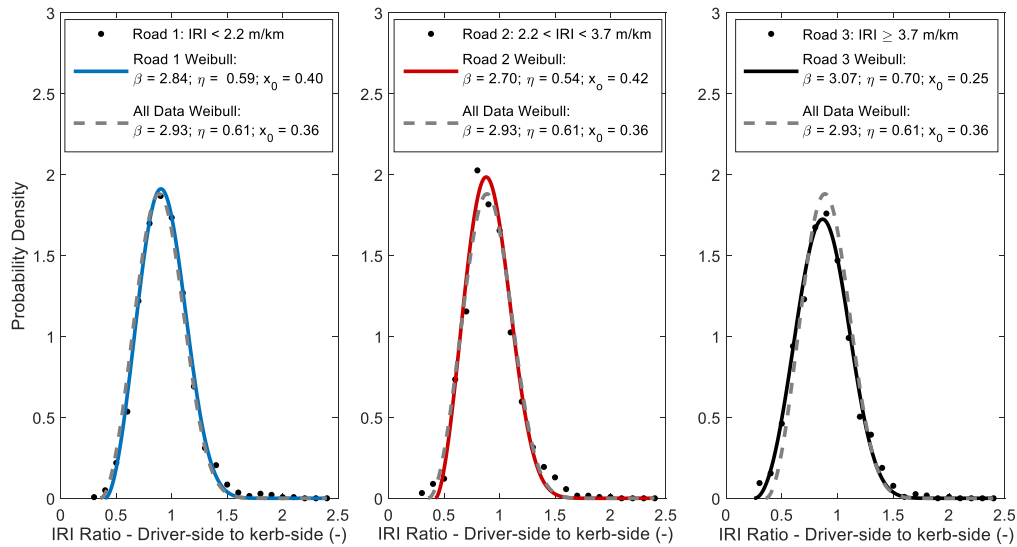


Figure 6: Probability density functions for ratio of driver-side to kerb-side wheel-track IRI.

Coherence relationship between the driver-side and kerb-side wheel tracks

Although the magnitude of the wheel-track roughness is correlated along the length of the data segment, the overall correlation function varies with spatial frequency. As discussed in the introduction, the most common approach for simulating dual wheel-track data is to use the coherence function between the driver-side and kerb-side wheel-tracks to establish the correlated and non-correlated portions of the signal. Lamb and Rouillard [19] found that the coherence function can be described by a single variable, b_l , in accordance with (1). By analysing the wheel-track data in short segments along the length of the road, Lamb and Rouillard were able to reveal the nonstationary nature of the coherence function and the distribution of b_l for sealed asphalt roads of any roughness (Figure 7). This distribution can be used to randomise the coherence function, which when combined with the technique presented by Long [14] can be used to generate realistically correlated, nonstationary dual wheel-track elevation data.

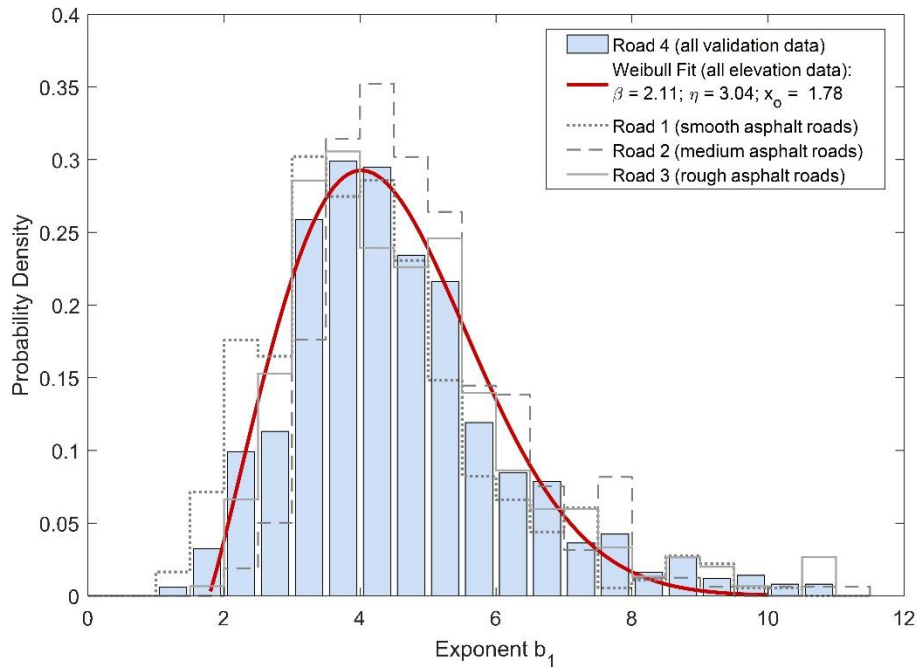


Figure 7: Probability density function of the exponent of the driver-side to kerb-side wheel-track coherence function [19].

Overall synthesis process

The discussions thus far have shown that three parameters describe the nonstationarity of road elevation profiles. Namely, these are the kerb-side track IRI, the driver-side to kerb-side track IRI ratio and the coherence function parameter, b_l . Statistical distributions for these parameters have all been characterised using the three parameter Weibull distribution. For the latter two cases, the Weibull function is fixed as the distributions were found not to vary significantly with road roughness (IRI), whereas the kerb-side track IRI distribution varies with the mean IRI and can be fully described by the scale parameter determined using (6).

The scheme for creating nonstationary dual-track longitudinal elevation profiles is discussed here and is based on the repeated generation of stationary dual track profile segments which are concatenated to produce a dual-track profile of the desired length. For each stationary segment, the IRI ratio and coherence between the driver-side and kerb-side tracks vary according to statistical distributions presented in Figures 6 and 7 respectively. The overall synthesis process is shown in Figure 8 and requires the following as its inputs:

- The desired kerb-side track IRI distribution by setting the mean IRI (from which the Weibull scale parameter is calculated - equation 6) in accordance with Table 3 to simulate a road of the desired nominal roughness.
- The dual track length to be synthesized
- The length of (stationary) segments
- The wheel track (nominally 1.5 m)

Once the inputs have been selected, the dual track profile for each stationary segment is generated and concatenated until the desired number of segments has been reached. It is important to note that each dual track segment will have different kerb-side and driver-side track roughness levels and driver-side

to kerb-side track coherence functions resulting in an overall nonstationary process that faithfully represents the random variation as exhibited by real roads.

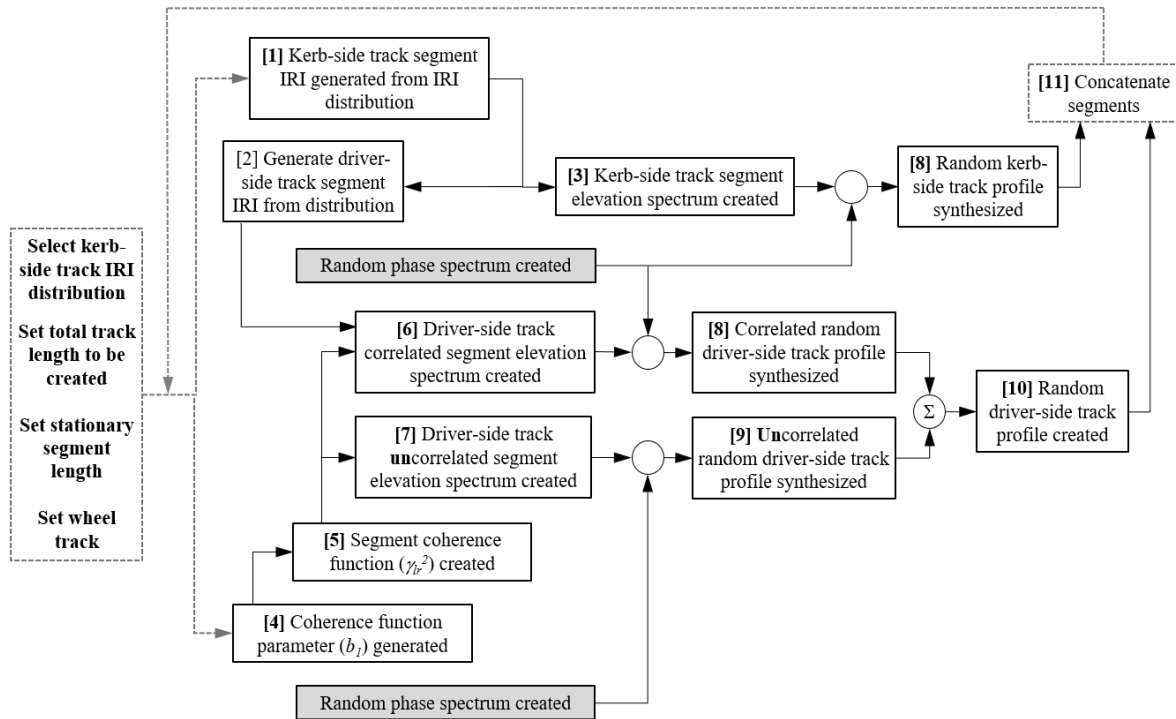


Figure 8. Nonstationary, dual track synthesis flowchart.

Explanatory notes for the flow chart shown in Figure 8 are given below:

- 1 The IRI level of the kerb-side track segment is randomly generated from the Weibull distribution of the IRI (equation 4) using a suitable linear congruential generator (such as the *wblrnd* function in Matlab® and applying an offset to represent the location parameter, x_o) [30].
- 2 The IRI level of the corresponding driver-side track is randomly generated from driver-side to kerb-side wheel track IRI ratio distribution (three parameter Weibull model with $x_o = 0.36$, $\beta = 2.93$ and $\eta = 0.61$) as shown in Figure 6 using the same technique as in step 1.
- 3 The kerb-side track segment elevation spectrum, based on the ISO 8608 model, is generated using equations (2) and (3).
- 4 The corresponding dual track coherence parameter, b_l for the segment is randomly generated from the parameter distribution (three parameter Weibull model with $x_o = 1.78$, $\beta = 2.11$ and $\eta = 3.04$) as shown in Figure 7 using the same technique as in step 1.
- 5 The coherence function for the segment is generated using equation (1).
- 6 The driver-side track correlated segment elevation spectrum is generated from the product of the kerb-side track elevation spectrum and the coherence function (spectrum) and adjusted for the driver-side to kerb-side track IRI ratio.
- 7 The driver-side track **uncorrelated** segment elevation spectrum is produced from the product of the kerb-side track elevation spectrum and the **incoherence** ($1 - \gamma_{lr}^2$) function (spectrum) and adjusted for the driver-side to kerb-side track IRI ratio.
- 8 The kerb-side track and correlated driver-side track elevation spectra are combined with a single uniformly-distributed random phase spectrum to produce the kerb-side track and correlated

driver-side track random elevation profiles for the segment respectively by using the inverse Fourier transform.

- 9 The **uncorrelated** driver-side track elevation spectrum is combined with a separate uniformly-distributed random phase spectrum to produce the **uncorrelated** driver-side track random elevation profile for the segment by using the Inverse Fourier transform.
- 10 The segment driver-side track elevation profile is obtained by summing the correlated and **uncorrelated** elevation profiles.
- 11 Both track segments are continually concatenated ensuring that discontinuities are eliminated by application of an appropriate windowing function (such as the Tukey window) to each synthesized segment.

Results

For the purpose of demonstrating the functionality of the algorithm, results for a rough road conforming to the distribution of road 3 of Lamb and Rouillard [19] were produced. The Weibull parameters were taken directly from Figure 2 which happens to closely match the distribution of roughness class BB. Alternatively a desired mean IRI can be set and the scale parameter calculated using equation 6 or the values from Table 3 can be applied directly.

The length of each segment was set to 100 m and the total number of segments to be synthesized was set to 250 (resulting in a 25 km long road). The wheel track was set to 1.5 m. The results are presented in Figure 9 and include the mean (indicated by the vinculum) and range of each parameter used to synthesize the dual track road profile. These include the roughness parameter $G_d(\Omega_o)$, the coherence parameter b_l , the kerb-side track IRI and the driver-side to kerb-side track IRI ratio. The roughness variation for each segment is evident in Figure 9(a), as is the (partial) correlation between the kerb-side and driver-side tracks.

The results in Figure 9(b) show that the average synthesized kerb-side track PSD (red line) is in good agreement with the target average PSD (black line). The grey dashed lines represent the range of the target PSD.

From Figure 9(c) it can be seen that agreement between the overall coherence function of the synthesized road (red line) and the overall target coherence function (black line) is also good. Again, the grey dashed lines represent the range of the target coherence function.

The variations in road roughness for the driver-side and kerb-side synthesized wheel tracks conform to the respective statistical distributions as shown in Figure 9(d) and Figure 9(e). The distributions from the synthesized elevation profiles are represented by the red bars whereas the target distributions as represented by the solid black line.

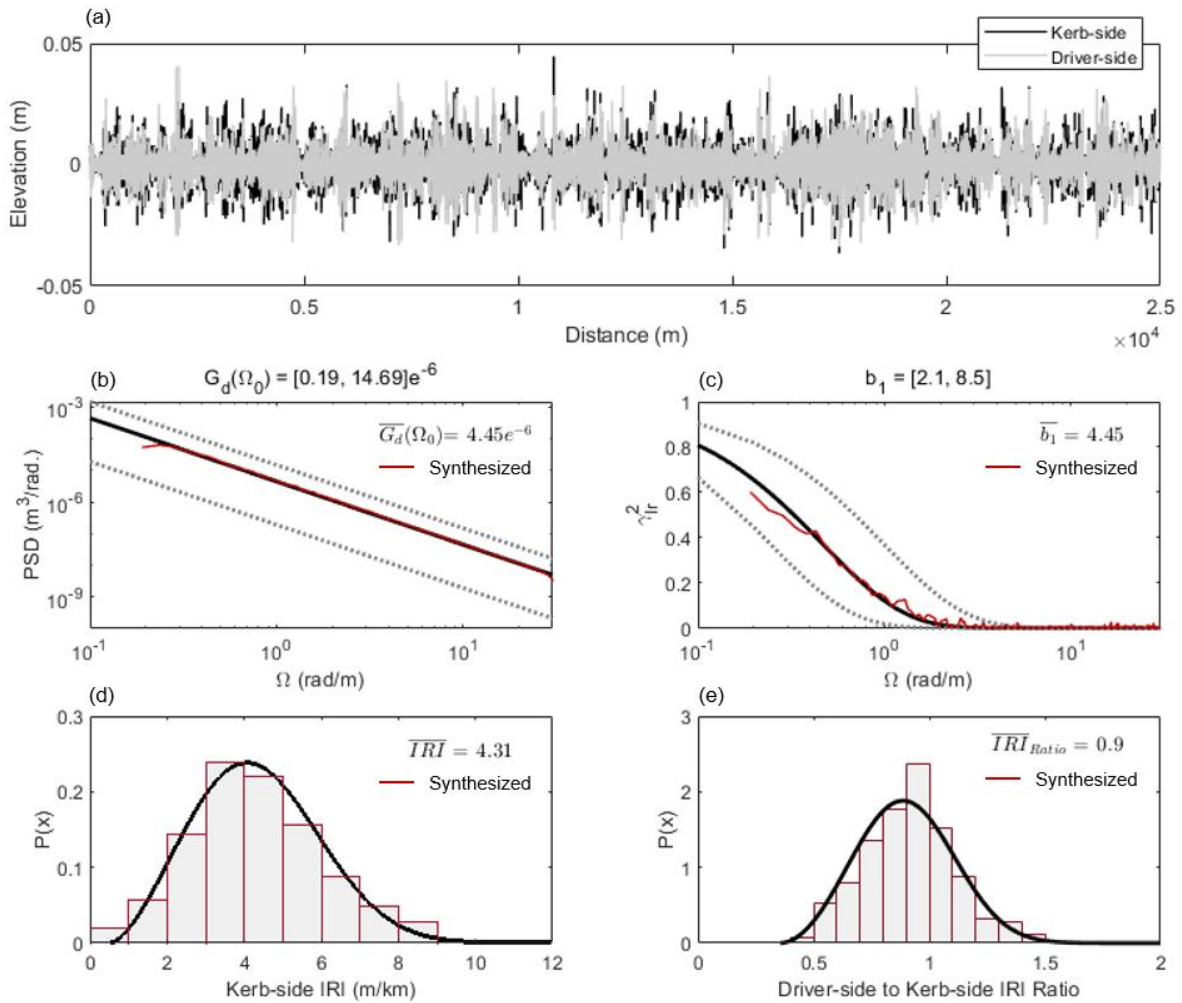


Figure 9: Example synthesis for rough roads using road 3 [19] IRI distribution. (a): synthesised elevations; (b): average and range of elevation PSD of kerb-side track; (c): average and range of coherence function; (d): kerb-side track IRI distribution; (e): driver-side to kerb-side track IRI ratio distribution.

Figure 10 shows a 100 m section straddling two adjacent segments to reveal the synthesised elevation data. The results show a correlation between the two tracks which decreases in strength as the wavelength is reduced which is a result of the driver-side to kerb-side track coherence function. Minor differences in the roughness of the two tracks is also evident, especially for the second 50 m section, which is a result of the independently-modulated driver-side to kerb-side IRI ratio. A smooth transition between adjacent segments is also evident and is achieved through the application of the Tukey window function.

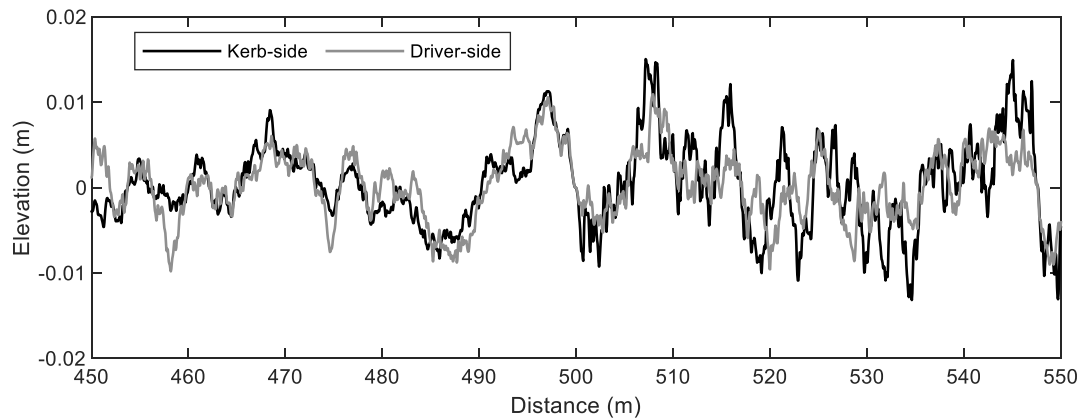


Figure 10: 100 m section showing details of the synthesized dual-track elevation profiles.

Conclusions

A novel method for synthesizing nonstationary dual wheel track longitudinal pavement elevation profiles was introduced. The longitudinal elevation signals are synthesized in a sequence of stationary segments and include independent random variations in road roughness and spectral content along the length of the wheel tracks. These stationary segments are concatenated to produce nonstationary dual track elevation data.

The variation in roughness of the kerb-side wheel track is defined by the three-parameter Weibull distribution with two fixed parameters (location and shape) thus affording simplicity for describing the distribution of road roughness with scale parameter alone. This was used to create a new roughness classification scheme to better represent the roughness range encountered on sealed roads in modern road networks. A random sequence of roughness values for the kerb-side track of the synthesized road is generated with a linear congruential generator from the Weibull distribution. The Weibull distribution was also used to describe the distribution of the road segment roughness ratio between two parallel wheel tracks. One interesting outcome of the paper is that this relationship appears independent of overall road roughness. This relationship is used to create the random sequence of roughness values for the driver-side track segments. The coherence function relating the two parallel wheel tracks is also made to vary randomly in accordance with previous findings [19]. This is achieved with the use of the Weibull model which describes the statistical distribution of the coherence parameter, b_l . For each stationary road segment, a different coherence function is used based on the random generation of the coherence parameter.

Results from the application of the new synthesis approach show that it is capable of producing dual wheel track elevation profiles that are nonstationary and replicate the natural (random) variations in road roughness and parallel track coherence that are found to exist on real roads.

Further work related to this research could include the analysis of the roughness ratio distribution and the dual track coherence variations for non-asphalt roads. Further, one alternative approach to characterising the relationship between the parallel tracks is to analyse the lateral road gradient as a single variable.

References

1. Cao, D., Song, X. and Ahmadian, M., 2011. Editors' perspectives: road vehicle suspension design, dynamics, and control. *Vehicle System Dynamics*, 49(1-2), pp.3-28.
2. La Barre, R.P., Forbes, R.T. and Andrew, S., 1969. The measurement and analysis of road surface roughness.
3. Dodds, C.J. and Robson, J.D. (1973). The description of road surface roughness. *Journal of Sound and Vibration*, 31(2), pp.175-183.
4. ISO Standards, 2016. *8608: 2016 Mechanical Vibration–Road Surface Profiles–Reporting of Measured Data*. BSI Standards Publication: London, UK.
5. Rouillard, V., Sek, M.A. and Bruscella, B., 2001. Simulation of road surface profiles. *Journal of Transportation Engineering*, 127(3), pp.247-253.
6. Steinwolf, A., Giacomini, J.A. and Staszewski, W.J., 2002. On the need for bump event correction in vibration test profiles representing road excitations in automobiles. *Proceedings of the Institution of Mechanical Engineers, Part D: Journal of Automobile Engineering*, 216(4), pp.279-295.
7. Abdullah, S., Giacomini, J.A. and Yates, J.R., 2004. A mission synthesis algorithm for fatigue damage analysis. *Proceedings of the Institution of Mechanical Engineers, Part D: Journal of Automobile Engineering*, 218(3), pp.243-258.
8. Yonglin, Z. and Jiafan, Z., 2006. Numerical simulation of stochastic road process using white noise filtration. *Mechanical Systems and Signal Processing*, 20(2), pp.363-372.
9. Bogsjö, K., 2007. Evaluation of stochastic models of parallel road tracks. *Probabilistic Engineering Mechanics*, 22(4), pp.362-370.
10. Bogsjö, K., Podgórski, K. and Rychlik, I., 2012. Models for road surface roughness. *Vehicle System Dynamics*, 50(5), pp.725-747.
11. Hongbin, R., Sizhong, C. and Zhicheng, W., 2011, August. Model of excitation of random road profile in time domain for a vehicle with four wheels. *In 2011 International Conference on Mechatronic Science, Electric Engineering and Computer (MEC)* (pp. 2332-2335). IEEE.
12. Feng, J., Zhang, X., Guo, K., Ma, F. and Karimi, H.R., 2013. A frequency compensation algorithm of four-wheel coherence random road. *Mathematical Problems in Engineering*.
13. Liu, X., Wang, H., Shan, Y. and He, T., 2015. Construction of road roughness in left and right wheel tracks based on PSD and coherence function. *Mechanical Systems and Signal Processing*, 60, pp.668-677.
14. Long, M.T., 2016. *On the statistical correlation between the heave, pitch and roll motion of road transport vehicles* (Doctoral dissertation, Victoria University).
15. Kamash, K.M.A. and Robson, J.D. (1977). Implications of isotropy in random surfaces. *Journal of Sound and Vibration*, 54(1), pp.131-145.
16. Ammon, D. (1992). Problems in road surface modelling. *Vehicle System Dynamics*, 20(sup1), pp.28-41.
17. Bogsjö, K. (2008). Coherence of road roughness in left and right wheel-track. *Vehicle System Dynamics*, 46(S1), pp.599-609.
18. Múčka, P. (2015). Model of coherence function of road unevenness in parallel tracks for vehicle simulation. *International Journal of Vehicle Design*, 67(1), pp.77-97.

19. Lamb, M.J. and Rouillard, V., 2020. Nonstationary coherence characteristics of dual track road profile data. *Mechanical Systems and Signal Processing*, 140, p.106721.
20. Múčka, P., 2017. International Roughness Index specifications around the world. *Road Materials and Pavement Design*, 18(4), pp.929-965.
21. Sayers, M.W. (1995). On the calculation of international roughness index from longitudinal road profile. *Transportation Research Record*, (1501).
22. Sayers, M.W. and Karamihas, S.M. (1998). *The little book of profiling: basic information about measuring and interpreting road profiles*.
23. Johannesson, P. and Rychlik, I. (2012). *Modelling of road profiles using roughness indicators*.
24. Sun, L., Zhang, Z. and Ruth, J., 2001. Modeling indirect statistics of surface roughness. *Journal of Transportation Engineering*, 127(2), pp.105-111.
25. Kropáč, O. and Múčka, P., 2005. Be careful when using the International Roughness Index as an indicator of road unevenness. *Journal of Sound and Vibration*, 287(4-5), pp.989-1003.
26. Pawar, P.R., Mathew, A.T. and Saraf, M.R., 2018. IRI (International Roughness Index): An Indicator of Vehicle Response. *Materials Today: Proceedings*, 5(5), pp.11738-11750.
27. Karamihas, S.M., Gilbert, M.E., Barnes, M.A. and Perera, R.W., 2019. *Measuring, characterizing, and reporting pavement roughness of low-speed and urban roads* (No. Project 10-93).
28. Murthy, D.P., Xie, M. and Jiang, R. (2004). *Weibull models* (Vol. 505). John Wiley & Sons.
29. Devroye, L., 2006. Nonuniform random variate generation. *Handbooks in operations research and management science*, 13, pp.83-121